STRUCTURAL SCIENCE
CRYSTAL ENGINEERING
MATERIALS

Volume 74 (2018)

Supporting information for article:

Structure factors and charge-density study of diamond at 800 K

Yuka Deguchi and Eiji Nishibori

S1. Powder profiles and intensity histograms in the back ground region at 300K.

Figure S1 shows the powder profiles and intensity histograms in the background regions at 300K. The profiles and histograms were created by using the same method as in the case of Figure 3. We estimated the standard deviations of the histograms. The histograms of first, second and third data could be expressed as a single Gaussian peak as shown in Figures S1 (*a*), S2 (*b*) and S3 (*c*). Random noises were dominant in these data. The histograms became broader with the increasing data number. These were consistent with the profiles at 800K.

S2. Fourier series expansion of powder profiles.

Figures S2 (*a*) and (*b*) show expanded regions around n=1300 of the Fourier series expansion of the sixth powder profile at 300K. Figures S2 (*a*) and S2 (*b*) show the amplitude of cosine term and the amplitude of sine term, respectively. There is sharp peak at n=1308, which corresponds to a six data-point step. Figures S2 (*c*) and S2 (*d*) show the expanded regions around n=1300 of the Fourier series expansion of the first, second, third, fourth and fifth powder profiles at 300K. Figures S2 (*c*) and S2 (*d*) show the amplitude of cosine terms and the amplitude of sine terms, respectively. Only the cosine terms of the fifth dataset exhibited small peaks, indicating a six-pixel cycle noise. No peaks were found in the other dataset. Figure S2 (*e*) shows the sum of each six-point of the background region for the fifth dataset. The random errors of the sum are greater than the intensity fluctuations.

S3. Fitting result of Rietveld refinement for sixth dataset at 800 K and 300 K.

Figures S3 (*a*), and S3 (*b*) show the fitting results of the Rietveld refinement for the uncorrected and the corrected data, respectively, at 800 K. The fluctuation of the green line decreased less than 50 % indicating the effectiveness of the correction. The R_{wp} and R_I in the sixth dataset were also decreased from 0.52 % to 0.48 % and from 2.86 % to 2.64 %. It should be noted that R_{wp} and R_I of more than 75º in 2θ were decreased more than 0.09 % and 3.19%, respectively, by the applied corrections.

Figures S3 (*c*) and S3 (*d*) show the fitting results of the Rietveld refinement for the uncorrected and corrected data, respectively, at 300 K. The fluctuation of the green line also decreased less than 50 % indicating the effectiveness of the correction. The R_{wp} and R_I in the sixth dataset were also decreased from 0.59% to 0.54% and from 2.41% to 2.37%. This fact indicates that the data in this region were available for the charge density study.

Intensity fluctuations by thermal diffuse scattering can also be recognized by the comparison of Figures S3 (*b*) and S3 (*d*). The fluctuations under the Bragg peaks can be considered as a thermal diffuse scattering. The corrected data enables us to analyse the thermal diffuse scattering at the $d \cong 0.2$ Å region. The corrected data were applied to the charge density study.

S4. Structure factors compared with the previous studies.

Table S1 listed the structure factors of the present and previous studies. The data measured and analysed by Brill (Brill, 1950) is denoted Brill. The powder data measured by Göttlicher & Wölfel is denoted BW. The powder data measure at SPring-8 (Nishibori et al., 2007) and Petra-III (Bindzus et al., 2014) are denoted as Nishibori and Bindzus. The data measured using the Pendellösung method (Takama et al., 1990) is denoted Takama. The first ten reflections of the present data at 300 K and the most recent study by Bindzus et al were well agreed with Takama's Pendellösung method dataset. The data below 311 of the GW data were approach to those of the present data at 800 K. Previous powder data GW, Nishibori et al, and Bindzun et al systematically deviated from the present data at 300 K in the higher reciprocal resolution region. The deviations of low resolution data were greater than those of the high resolution data.

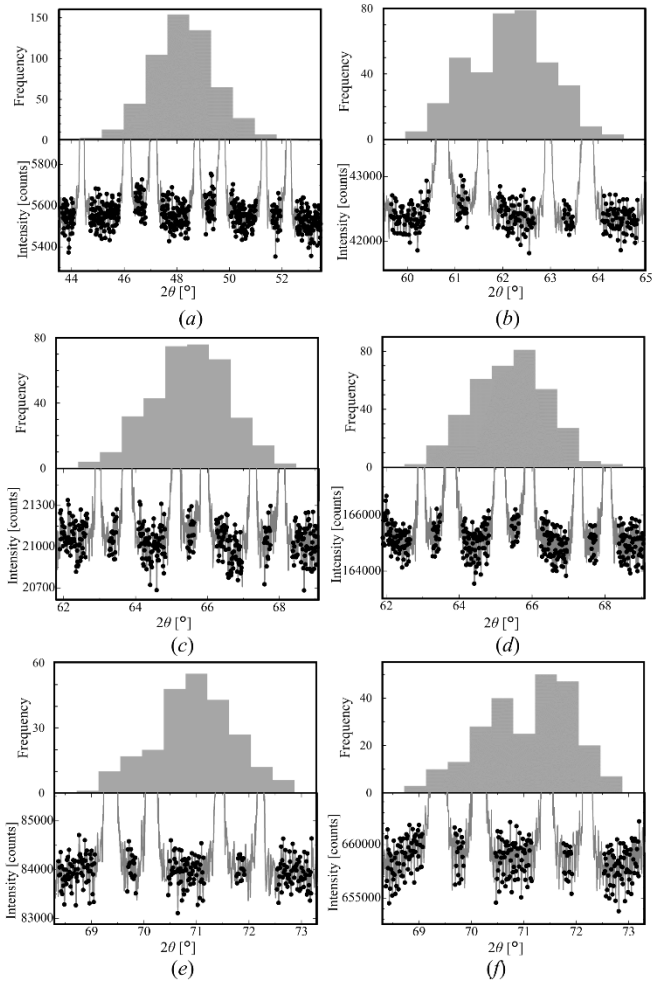

Figure S1 Powder profiles and intensity histograms in the background regions at 300 K.

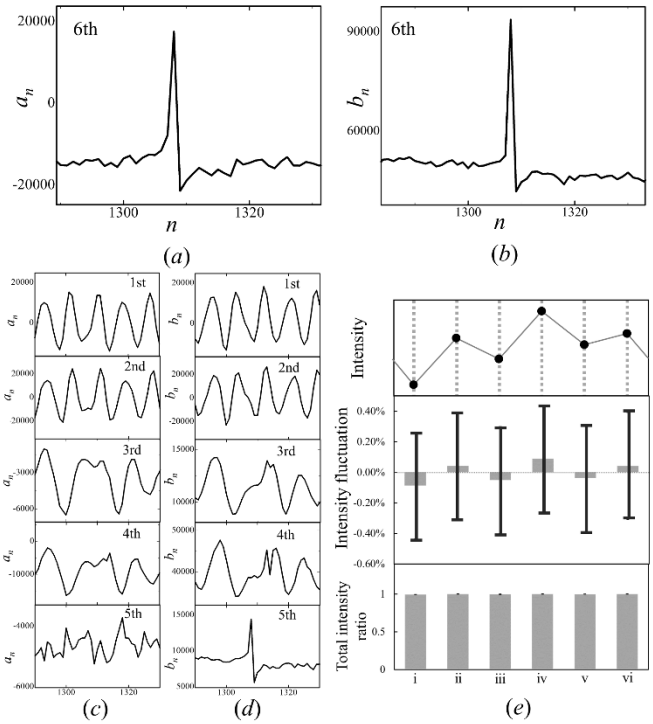

Figure S2 Expanded regions around n=1300 of the Fourier series expansions of the powder profiles. Amplitudes of (*a*) cosine and (*b*) sine terms of the sixth powder profiles at 300K. Amplitudes of (*c*) cosine and (*d*) sine terms of first, second, third, fourth and fifth powder profiles at 800K and 300K.

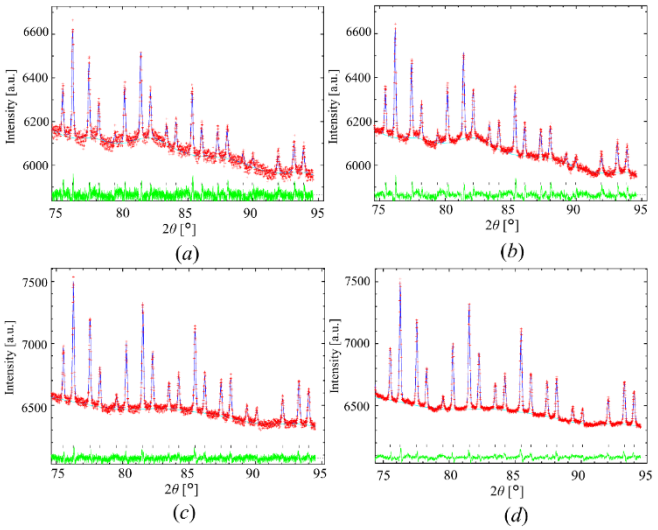

Figure S3 Fitting results of the Rietveld refinement for the (*a*) uncorrected and (*b*) corrected data at 800 K. Fitting results of the Rietveld refinement for the (*c*) uncorrected and (*d*) corrected data at 300K.

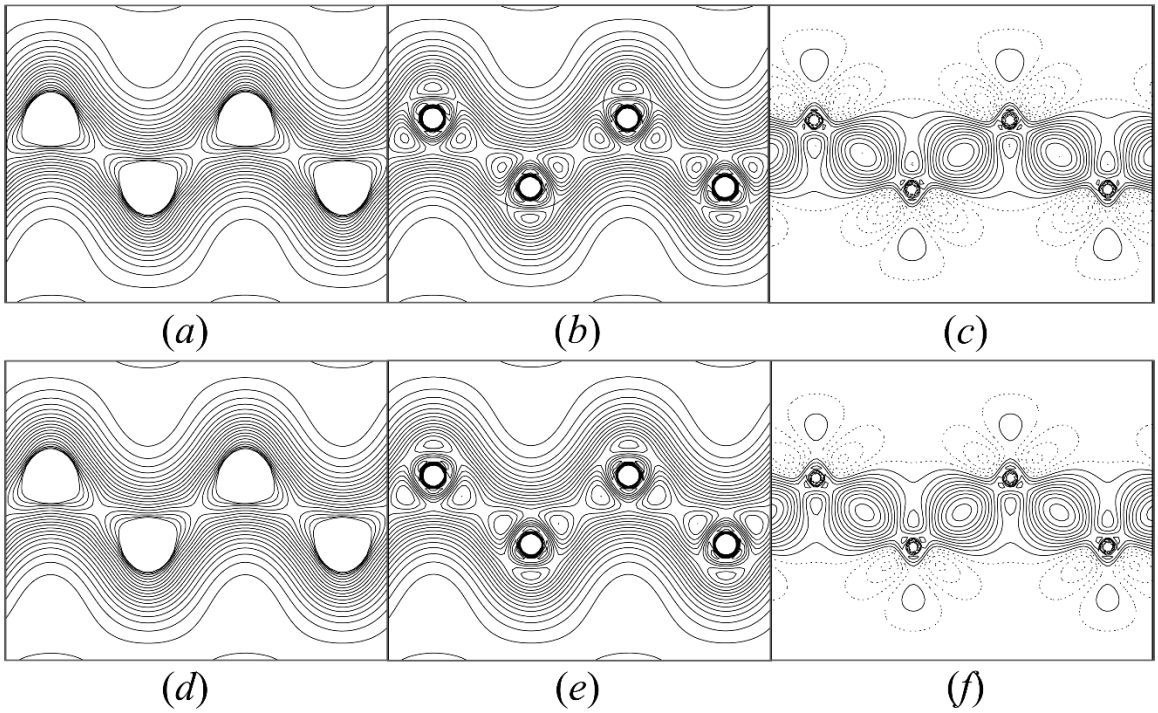

Figure S4 Charge density maps for the 1 1 0 plane at 800 K and 300 K: (*a*) total, (*b*) valence, and (*c*) static deformation maps at 800K and (*d*) total, (*e*) valence, and (*f*) static deformation maps at 300K. Contour lines were drawn from 0.0 e/Å^3 to 2.0 e/Å^3 with 0.1 e/Å^3 step width for (*a*), (*b*), (*d*), and (*e*) and from –0.5 e/Å^3 to 0.6 e/Å^3 with 0.05 e/Å^3 step width for (*c*) and (*f*).

Table S1 The list of structure factors of the present and previous studies. The data measured and analysed by Brill (Brill, 1950) are denoted Brill. The powder data measured by Göttlicher & Wölfel are denoted BW. The powder data measured at SPring-8 (Nishibori et al., 2007) and Petra-III (Bindzus et al., 2014) are denoted as Nishibori and Bindzus.

h k l	800K	300K	Brill	GW	Takama	Nishibori	Bindzus
1 1 1	18.123(6)	18.205(6)	18.664	18.57(4)	18.37(6)	18.13(2)	18.6(19)
2 2 0	15.016(8)	15.223(8)	14.44	15.29(7)	15.36(5)	15.13(2)	15.4(15)
3 1 1	9.006(7)	9.196(7)	8.480	9.01(4)	9.32(3)	9.07(2)	9.23(9)
2 2 2	0.97(6)	0.9(10)	1.104			1.0(2)	0.88(5)
4 0 0	11.78(16)	11.99(16)	11.048	11.11(7)	11.93(3)	11.73(5)	11.9(12)
3 3 1	8.208(9)	8.435(9)	7.776	8.29(3)	8.39(3)	8.30(2)	8.38(8)
4 2 2	10.44(10)	10.82(10)	9.328	10.50(16)	10.9(3)	10.61(3)	10.8(11)

5	1	1	7.06(11)	7.39(11)	6.800	7.21(3)	7.41(3)	7.12(3)	7.26(7)
3	3	3	6.85(18)	7.22(18)	6.680	7.21(3)	7.28(2)	7.09(5)	7.20(7)
4	4	0	9.29(16)	9.83(16)	8.960	9.08(7)	9.58(2)	9.56(4)	9.8(10)
5	3	1	6.318(9)	6.66(8)		6.26(17)		6.45(2)	6.54(7)
6	2	0	8.29(13)	8.88(13)		8.35(4)		8.51(3)	8.69(9)
5	3	3	5.65(13)	6.09(13)	5.720	5.70(3)		5.89(4)	5.97(6)
4	4	4	7.47(2)	8.14(2)	7.128			7.79(7)	7.87(8)
7	1	1	5.04(15)	5.47(15)	5.096	5.07(17)		5.26(4)	5.38(6)
5	5	1	5.06(15)	5.49(15)	5.096	5.07(17)		5.26(4)	5.40(6)
6	4	2	6.70(10)	7.33(10)		6.76(2)		7.04(3)	7.20(7)
7	3	1	4.56(11)	5.03(11)		4.58(5)		4.78(4)	4.90(5)
5	5	3	4.52(15)	5.00(15)	4.464	4.58(5)		4.77(9)	4.89(5)
8	0	0	6.01(3)	6.68(3)	6.208			6.37(3)	6.45(9)
7	3	3	4.06(16)	4.55(17)	4.200			4.37(4)	4.44(5)
8	2	2	5.46(16)	6.07(17)	5.584	5.58(3)		5.79(6)	5.91(6)
6	6	0	5.44(2)	6.06(2)	5.728	5.58(3)		5.76(3)	5.91(6)
7	5	1	3.68(3)	4.20(12)		3.76(3)		3.95(5)	4.06(4)
5	5	5	3.71(12)	4.18(3)	3.760	3.76(3)		3.91(8)	4.07(4)
8	4	0	4.86(18)	5.57(17)				5.25(5)	5.39(6)
7	5	3	3.31(12)	3.83(13)		3.44(2)		3.61(3)	3.72(4)
9	1	1	3.30(18)	3.82(18)	3.672	3.44(2)		3.60(5)	3.71(4)
6	6	4	4.43(18)	5.09(19)	4.752			4.79(5)	4.96(6)
9	3	1	3.02(13)	3.52(13)				3.29(4)	3.37(4)
8	4	4	4.00(19)	4.67(19)	4.264			4.41(5)	4.56(6)
7	7	1	2.71(2)	3.20(19)	3.208			2.98(5)	3.11(4)
9	3	3	2.71(2)	3.20(19)	3.248			2.98(5)	3.11(4)
7	5	5	2.71(19)	3.19(19)	3.248			2.98(5)	3.10(4)
10	2	0	3.60(19)	4.29(2)				4.02(5)	4.16(4)
8	6	2	3.62(14)	4.30(14)				4.04(5)	4.16(4)
7	7	3	2.49(2)	2.96(2)	2.912			2.73(5)	2.88(4)

9	5	1	2.51(14)	2.98(13)			2.73(4)	2.88(4)
9	5	3	2.29(15)	2.72(15)				2.60(4)
10	4	2	3.01(15)	3.69(15)				3.52(4)
11	1	1	2.09(2)	2.51(2)	2.320			2.43(4)
7	7	5	2.10(2)	2.52(22)	1.736			2.43(4)
8	8	0	2.83(3)	3.38(3)	2.872			3.3(11)
11	3	1	1.88(16)	2.31(15)				2.25(3)
9	7	1	1.88(16)	2.30(15)				2.25(3)
9	5	5	1.87(2)	2.30(2)	1.920			2.25(3)
10	6	0	2.51(2)	3.14(2)				3.00 (5)
8	6	6	2.51(2)	3.14(2)	2.392			3.00(5)
11	3	3	1.70(2)	2.18(2)	1.176			2.05(4)
9	7	3	1.72(15)	2.19(16)				2.05(4)
12	0	0	2.34(4)	2.85(5)				2.78(6)
8	8	4	2.36(2)	2.87(2)				2.78(6)
11	5	1	1.59(15)	2.01(15)				1.90(5)
7	7	7	1.57(4)	1.99(4)				1.90(5)
12	2	2	2.07(2)	2.67(2)				
10	6	4	2.08(17)	2.68(17)				
11	5	3	1.46(17)	1.81(17)				
9	7	5	1.45(17)	1.81(17)				
12	4	0	1.98(2)	2.54(2)				
9	9	1	1.34(2)	1.82(2)				
10	8	2	1.77(17)	2.32(17)				
13	1	1	1.21(3)	1.59(3)				
9	9	3	1.21(3)	1.59(3)				
11	7	1	1.22(16)	1.59(16)				
11	5	5	1.21(3)	1.59(3)				
12	4	4	1.72(2)	2.13(2)				
9	7	7	1.11(2)	1.50(2)				

11	7	3	1.11(18)	1.51(16)
13	3	1	1.11(18)	1.51(17)
12	6	2	1.56(15)	2.08(17)
13	3	3	1.11(3)	1.36(3)
9	9	5	1.11(3)	1.36(3)
8	8	8	1.39(4)	2.14(4)
11	7	5	1.01(19)	1.31(19)
13	5	1	1.01(19)	1.31(19)
14	2	0	1.28(2)	1.79(3)
10	10	0	1.27(4)	1.79(4)
10	8	6	1.28(19)	1.80(16)
13	5	3	0.91(16)	1.21(17)
11	9	1	0.91(16)	1.21(17)
12	8	0	1.17(3)	1.67(2)
9	9	7	0.87(2)	1.18(3)
11	9	3	0.88(16)	1.18(16)
14	4	2	1.13(17)	1.55(2)
10	10	4	1.13(3)	1.54(3)
12	6	6	1.13(3)	1.54(3)
11	7	7	0.75(3)	1.07(3)
13	7	1	0.77(19)	1.07(19)
13	5	5	0.75(3)	1.07(2)
12	8	4	1.07(18)	1.52(19)
15	1	1	0.73(3)	0.98(3)
13	7	3	0.73(19)	0.99(2)
11	9	5	0.73(19)	0.99(2)
14	6	0	0.86(3)	1.47(3)
15	3	1	0.77(16)	0.98(2)
11	11	1	0.66(3)	0.94(3)

13	7	5	0.68(2)	0.94(2)
9	9	9	0.65(4)	0.93(5)
15	3	3	0.66(3)	0.94(3)
14	6	4	0.83(18)	1.21(2)
12	10	2	0.83(18)	1.21(2)
13	9	1	0.57(17)	0.83(18)
11	11	3	0.56(3)	0.83(2)
11	9	7	0.57(17)	0.83(18)
15	5	1	0.56(17)	0.83(18)

Table S2 Final parameters of multipole modelling.

T [K]	800 K					
a [Å]	3.57192(1)					
Model	C	C anh	Cv	Cv anh	C EHC	C EHC anh
R/WR (%)	0.86/ 0.40	0.79/ 0.35	0.83/ 0.38	0.90/ 0.41	0.79/ 0.36	0.79/ 0.35
GOF	1.8362	1.6343	1.7267	1.8701	1.6240	1.5811
u^2_{iso} (Å^2)	0.00280(14)	0.00292(5)	0.00263(14)	0.00249(5)	0.0026(8)	0.0030(8)
κ	0.971(3)	0.965(4)	0.937(3)	0.946(5)	0.962(5)	0.97(10)
κ'	0.94(12)	0.94(11)	0.89(11)	0.90(12)	0.934(9)	0.94(11)
*O*2-	0.0156(3)	0.0157(2)	0.0176(3)	0.0176(3)	0.0155(2)	0.0157(13)
*H*0	-0.0015(4)	-0.0016(4)	-0.0032(6)	-0.0027(6)	-0.0016(3)	-0.0016(3)
P_v	0.1667	0.1667	0.1667	0.1667	0.1667(3)	0.1666(3)
κ_c	1.00	1.00	1.00	1.00	0.976(9)	1.01(6)
P_c	0.0833	0.0833	0.0833	0.0833	0.0833(3)	0.0834(3)
*C*123	0.00	0.00008(7)	0.00	0.00006(8)	0.00	0.00008(7)
*D*1111	0.00	0.00020(9)	0.00	-0.00023(9)	0.00	0.0003(5)
*D*1122	0.00	0.00007(3)	0.00	-0.00008(4)	0.00	0.0001(17)
$\rho(\mathbf{r})_{BCP}$ (eÅ^{-3})	1.662	1.663	1.673	1.673	1.655	1.664

$\nabla^2\rho(\mathbf{r})_{BCP}$ (eÅ^{-5})	-12.448	-12.732	-14.269	-13.944	-12.694	-12.750
$\lambda_3\rho(\mathbf{r})_{BCP}$ (eÅ^{-5})	9.41	9.06	7.42	7.88	8.85	9.11
$\nabla^2\rho(\mathbf{r})_{BCC}$ (eÅ^{-5})	-28.3	-28.2	-23.9	-24.3	-26.5	-28.6

300 K				
3.56750(1)				
C	C anh	Cv	Cv anh	C EHC
0.67/ 0.33	0.68/ 0.34	0.91/ 0.45	0.95/ 0.45	0.67/ 0.34
1.5531	1.6113	2.0836	2.1324	1.5833
0.00174(10)	0.00172(3)	0.00158(14)	0.00131(5)	0.0018(10)
0.969(2)	0.970(3)	0.931(4)	0.948(5)	0.97(15)
0.91(11)	0.91(11)	0.86(13)	0.87(14)	0.91(6)
0.0147(2)	0.0146(2)	0.0164(4)	0.0164(4)	0.0143(3)
-0.0030(4)	-0.0030(5)	-0.0054(9)	-0.0044(8)	-0.003(10)
0.1667	0.1667	0.1667	0.1667	0.167(5)
1.00	1.00	1.00	1.00	1.00(15)
0.0833	0.0833	0.0833	0.0833	0.083(5)
0.00	-0.00001(6)	0.00	-0.00002(8)	0.00
0.00	-0.00001(7)	0.00	-0.00039(8)	0.00
0.00	-0.00002(3)	0.00	-0.00015(3)	0.00
1.644	1.641	1.647	1.649	1.637
-12.243	-12.156	-13.867	-13.316	-12.048
9.02	9.08	6.97	7.85	9.08
-26.2	-26.2	-21.7	-22.3	-26.2